Autonomous solutions for powering wireless sensor nodes in rivers

E. Kamenar *[ab], S. Maćešić [a], G. Gregov [a], D. Blažević [ab], S. Zelenika [ab], K. Marković [ab], V. Glažar [a]
[a] University of Rijeka, Faculty of Engineering, Vukovarska 58, 51000 Rijeka, CROATIA
[b] Centre for Micro and Nano Sciences and Technologies, R. Matejčić 2, 51000 Rijeka, CROATIA

ABSTRACT

There is an evident need for monitoring pollutants and/or other conditions in river flows via wireless sensor networks. In a typical wireless sensor network topography, a series of sensor nodes is to be deployed in the environment, all wirelessly connected to each other and/or their gateways. Each sensor node is composed of active electronic devices that have to be constantly powered. In general, batteries can be used for this purpose, but problems may occur when they have to be replaced. In the case of large networks, when sensor nodes can be placed in hardly accessible locations, energy harvesting can thus be a viable powering solution. The possibility to use three different small-scale river flow energy harvesting principles is hence thoroughly studied in this work: a miniaturized underwater turbine, a so-called 'piezoelectric eel' and a hybrid turbine solution coupled with a rigid piezoelectric beam. The first two concepts are then validated experimentally in laboratory as well as in real river conditions. The concept of the miniaturised hydro-generator is finally embedded into the actual wireless sensor node system and its functionality is confirmed.

Keywords: wireless networks, pollution sensors, miniature hydro-generators, piezoelectric energy harvesting

1. INTRODUCTION

In recent times a need has arisen for enabling autonomous powering of wireless sensor network nodes that are, in fact, small computing devices designed specifically to perform simple measurement tasks. In a typical wireless sensor network topography, large arrays of sensor nodes are to be deployed in the environment, all wirelessly connected to each other (sensor nodes with relaying capabilities) and/or their gateways. Network nodes are employed to assess different values in the environment such as ambient temperature, pressure or humidity or even more complex parameters, such as the concentrations of certain pollutants. Sensors can and may be placed anywhere where it specifically suits the network topography, which means that sometimes, once installed, they can be hard to access. Moreover, since the traditional means of powering the sensor nodes is to use batteries that have a limited lifetime, a significant problem with their replacement occurs. Different energy harvesting principles, especially if combined with low consumption electronics and corresponding power management circuitry, linked with rechargeable batteries or supercapacitors, represent a way to overcome these limitations. Wireless sensor networks and the new 'Internet of things' (IoT) paradigm constitute then the primary drivers of energy harvesting technologies and smart energy conversion materials of the future.

The aim of this paper is to present the part of the work on the EU FP7 research project GOLDFISH, which is related to the design, manufacturing, validation and operation of an energy harvesting device, which enables the required autonomy of clusters of river-based pollution monitoring sensors. The sensors are part of an integrated system aimed at collecting, processing and transmitting pollution data to gateways located on the riverbank. Each gateway covers sensor clusters deployed in its communication range and delivers the collected data to the mainframe [1].

Although energy harvesting has been adopted in several applications and can rely of different energy conversion principles, from photovoltaics to thermoelectrics [2-5], small-scale river flow energy harvesting concepts have not yet been thoroughly investigated. Three different energy harvesting concepts, specifically designed for sensor nodes that are to be placed in watercourses, are hence explored in this work: a miniaturized underwater DC hydro-generator, a so-called 'piezoelectric eel' and a hybrid turbine solution coupled with a rigid piezoelectric beam (Fig. 1). The needed conditioning and management electronics, used to regulate harvester's voltage levels and keep them compatible with the foreseen loads, is also designed and optimized. The foreseen autonomous sensor nodes are to be placed at about 0.5 m from the bottom of the riverbed and used for measuring the concentration of pollutants present in the river flow. The in-flow sensors are to be

* ekamenar@riteh.hr; phone +385 51 651585; fax +385 51 651416; www.riteh.uniri.hr, www.cmnzt.uniri.hr & precenglab.riteh.uniri.hr

Smart Sensors, Actuators, and MEMS VII; and Cyber Physical Systems, edited by José Luis Sánchez-Rojas, Riccardo Brama, et. al., Proc. of SPIE Vol. 9517, 951712 · © 2015 SPIE
CCC code: 0277-786X/15/$18 · doi: 10.1117/12.2178250

deployed from 1 to 6 km apart from each other, with dedicated gateways, used to collect the data acquired by each sensor node, placed on the riverbank [1].

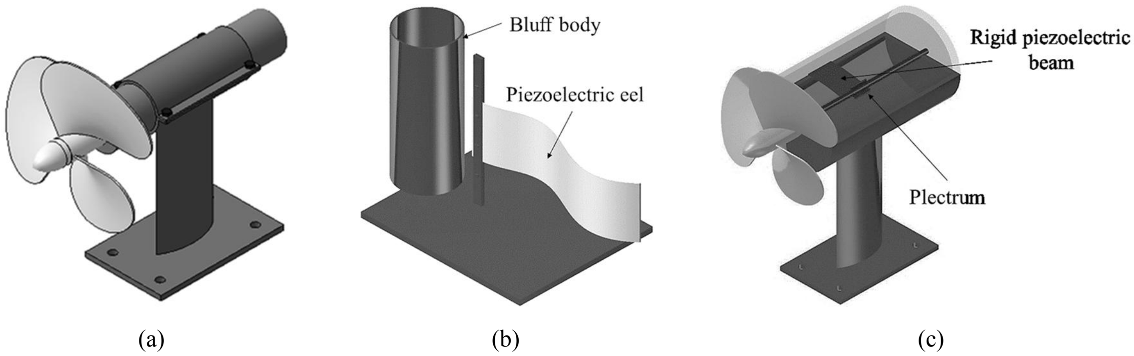

Figure 1: Principles of considered energy harvesting solutions: hydro-generator (a), piezoelectric eel (b) and 'plucked' piezoelectric beam (c).

The developed underwater hydro-generator concept [6] is fully tested in laboratory conditions and integrated within the autonomous wireless sensor node in real river conditions during the final testing phases of the GOLDFISH project in Poland. In the case of the piezoelectric eel energy harvesting concept, the optimized piezoelectric eel shapes, positions and bluff body dimensions, obtained via a custom-made C++ software based on the penalty immersed boundary method coupled to advanced optimization routines, are presented and discussed. The eels are then prototyped, based also on previous work [7-11], and experimentally tested in a flow tunnel at the Naval Research Institute in Zagreb, Croatia. The concept of a hybrid of the hydro-generator and a piezoelectric cantilever scavenger, which employs the plucking mechanism previously reported in literature [12], is numerically explored by employing a finite element coupled 3D analysis in ANSYS® [13]. A transient analysis is performed to simulate the system behaviour and obtain the voltage response allowing the generated powers to be estimated.

2. RIVER FLOW ENERGY HARVESTING CONCEPTS

Energy harvesting of river flows is especially suitable for powering wireless network sensor nodes that are to be placed in the river itself or on the riverbank. In this section, three small-scale river flow energy harvesting principles, to be used in powering pollution monitoring sensor nodes, are explained in detail: a miniaturized hydro-generator, a so called 'piezoelectric eel' and a hybrid turbine solution coupled with a piezoelectric beam (Fig. 1). The miniaturized underwater hydro-generator concept is based on a small direct current (DC) generator that is enclosed in a watertight brass enclosure. The propeller, used to convert the water-flow energy into a rotational action, is designed by using a 3D modelling software and printed on a 3D printer (Fig. 1a). The piezoelectric eel (Fig. 1b) is a composite flag-like compliant device made of two layers of piezoelectric polymer PVDF, one central polymer substrate layer and electrodes placed on PVDF's surfaces. This device is to be placed in a river stream behind a bluff body that induces Karman vortex street effects coercing the eel to move in a flapped motion that is converted into usable voltage for powering the foreseen loads. For the design of the eel, a custom software, that implements the penalty immersed boundary method, is developed in C++ and coupled with optimisation routines. This allows the dimensions of the ell, of the bluff body and of the respective distance to be thoroughly investigated. The eel is then prototyped and its performances are assessed experimentally. The third proposed harvesting configuration is a hybrid solution that is based on the concept of 'plucking' a rigid piezoelectric bimorph cantilever. In this case, the cantilever beam, enclosed in a suitable watertight enclosure, is plucked by means of several fulcrums protruding from propeller's shaft and then released allowing it to vibrate freely (Fig. 1c) thus generating, via the piezoelectric effect, electrical charge. The concept is modelled via a finite element model by using the ANSYS® software and its behaviour is simulated in a transient analysis routine with the excitation profile programmed in MATLAB®.

2.1. A miniaturized hydro-generator concept

Miniature energy harvesters based on a small DC generator and a propeller, although a well-examined concept on a macro scale, have not been used thus far to power low consumption wireless sensor nodes. The design of the miniaturised hydro-generator in the framework of the present research is based on considerations related to the power levels required by the load i.e. the sensor cluster constituted by the pollution sensor(s), by the respective electronics (so called measurement and controller boards) and the processing unit, as well as to the expected river conditions within the GOLFISH project [1]. Different designs variants are considered until an optimal version of the device is obtained [6, 14-15]. As depicted in Fig. 2, the considered concept is based on a conventional DC generator (1) rotated via the river flow by a propeller (2). The DC generator is coupled with the propeller shaft (3) by using an elastic coupling (4), while the shaft is held and centred via a bearing (5). A ring (6) mounted on the propeller shaft enables sealing of the turbine enclosure (7) composed of three parts and manufactured from brass due to its good anticorrosive properties. A cable feedthrough (8) completes the assembly [6].

The first assumption in hydro-generator design is the fact that it will be deployed in the river with flow velocities of up to 4 m/s. Since the voltage generated by the turbine increases with the third power of the flow velocity [14], it is not possible to choose a single miniaturized DC generator which can cover the wide foreseen range of the flow velocities. Four generators of the same type, but with different gearheads [16], are thus considered as a viable solution. With respect to the conditions related to the foreseen river experiments in Croatia and Poland (c.f. section 5), a Faulhaber 2233B018S generator with a 28:1 reduction ratio gearhead, which can cover a range of river velocities v_r = 0.5-1 m/s, is chosen in the first instance; its main characteristics are reported in Table 1. On the other hand, prior to experimental investigations, a rough verification of turbine blades performances is performed via numerical analysis with the aim of determining the propeller shape and dimensions [6]. The propeller is then designed based on further MATLAB® simulations allowing the optimal value of its diameter of d = 150 mm to be calculated. The propeller is finally printed in the ABS thermoplastic material on a Stratasys Fortus 250mc 3D printer [17]. In the final design configuration, the underwater hydro-generator has hence overall dimensions of 150 mm x 180 mm.

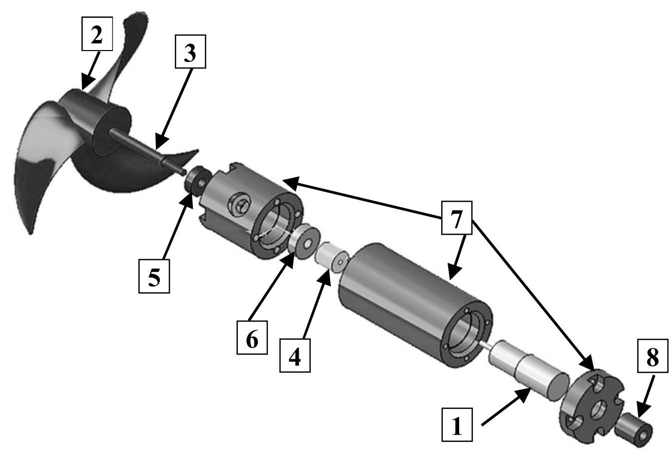

Figure 2. Hydro-generator assembly.

Table 1. Characteristics of the DC generator used in the experiments.

Device model	Output power	Nominal voltage	Gearhead type and reduction ratio	River flow coverage range
Faulhaber 2233B018S	P = 3.19W	U_n = 18 V	22E, i = 28:1	v_r = 0.5-1 m/s

2.2 The piezoelectric eel concept

In the past, several concepts for low-level energy harvesting of fluid (air or water) flows have been suggested. These are mainly based on the conversion of the flow energy via piezoelectric materials (i.e. via the direct piezoelectric effect). In this frame, solutions based on ceramic piezoelectric cantilevers [18], ceramic piezoelectric cantilevers with cylindrical extensions [19], polymer piezoelectric cantilevers coupled with a flexible diaphragm [20], piezoelectric polymer jellyfish [21] and the piezoelectric polymer eel concept, getting the most attention in the research community [7-11], have been investigated. Piezoelectric eels are compliant composite membrane devices that are placed in the rill of a bluff body located in a fluid flow (Fig. 1b). Depending on fluid velocity and the size and shape of the bluff body, the bluff body induces von Karman vortex street effects that cause the flapping of the piezoelectric membrane placed behind it. The membrane is hence coerced to flutter in an eel-like motion thus generating alternating electric charges on the surfaces of the piezoelectric polymer layers. The accumulated electric charge is drained by the electrodes covering the piezoelectric surfaces and the resulting voltage can therefore be fed into an energy harvesting/conditioning circuit.

The herein considered eel designs are based on the polyvinylidene fluoride (PVDF) polymer with excellent mechanical and piezoelectric properties [22]. In fact, PVDF is a lightweight engineering plastic material with high moisture resistance (< 0.02% moisture absorption) and high flexibility (with elongations of up to $\varepsilon \leq 50$ %) that can be shaped into any design and glued with most commercial adhesives. It is mechanically durable (with a yield strength of $\sigma_{0.2}$ = 55 MPa and Young's modulus of E = 2-4 GPa) and has a high elastic compliance (up to 10 times that of ceramic materials). When compared to other piezoelectric polymers in terms of the piezoelectric coefficient d, it surpasses most of them by an order of magnitude ($d_{31} \approx 20$ pC/N), while the usual values of its electromechanical coupling factor κ are around 10%. Additionally, any electrode pattern can be easily deposited onto its surface either by employing sputtering or a screen-printing processes.

The available published research about the piezoelectric eel concept delineates a strong dependence of the maximum produced output powers on several variables: river flow velocity v_r, bluff body shape and size, eel dimensions (including the number of electrode segments) and distance of the eel from the bluff body. It would also seem that an optimal solution, where the vortex shedding frequency matches that of the eel mode shapes, can be obtained only in a very narrow range of these variables.

A practical solution that would allow eel's constant fluttering while the sensor cluster is in its sleep mode, thus gathering enough energy for the foreseen measurements, is sought in the framework of the present work. A harvester solution for a variable river flow velocity and a number of designed variables with not-so-strict constraints is thus aimed for. Therefore, a suitable 2D model is custom-built in C++ by employing the penalty immersed boundary method where fluid flow is modelled using Navier-Stokes equations for an incompressible viscous fluid. To decrease computational intensity related to the case of the fluid encountering a massive membrane, the eel is then modelled as two separate beams: one massless, which interacts with the fluid (moves with it and exerts an external force onto it), and a second massive, which is connected to the first one with stiff springs [23, 15]. This 2D model simulates the formation of the von Karman vortex street occurring in the rill of the bluff body, as well as the interaction of the vortices with the piezoelectric membrane (Fig. 3). Based on the model, a preliminary optimisation of eel's shape, position and bluff body dimensions, at a chosen river flow velocity of v_r = 1 m/s, in which the objective function is maximizing eel's voltage output, is then performed by employing the GoSUMD software by AIMdyn Inc. [24]. The GoSUMD software is a tool for producing sampling points, evaluating global uncertainties and contributions of a large number of uncertain parameters to the model outputs, while enabling simultaneous examination of a vast number of effects on the outputs of interest. It is based on some of the fastest available computational algorithms for nonlinear model representation and sampling [25]. In the actual case of eel's concept, the optimisation is performed by using the mesh adaptive direct search algorithm for mixed variables [26].

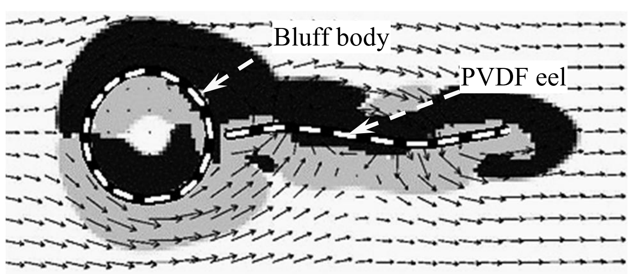

Figure 3. Numerical simulation of the dynamics of the piezoelectric eel in the rill of the bluff body.

The optimization is performed in two runs: in the first run, four electrode segments are considered regardless of the length of the eel, while in the second one fixed length (5 cm) electrode segments are placed along eel's length. The input parameters chosen for the optimization runs are the length L of the eel, the radius R of the bluff body and the distance d of eel's clamped end from the bluff body. During the optimisation runs, the parameters are chosen in the following ranges (expressed in meters): $L \in [0.20, 1.00]$, $R \in [0.05, 0.2]$, $d \in [0.02, 0.15]$ in the first run, and $L \in [0.20, 1.00]$, $R \in [0.1, 0.3]$, $d \in [0.05, 0.2]$ in the second run. What is more, all model input parameters have continuous uniform distributions and one hundred quasi-random samples are chosen in each run from the input parameter ranges, while the resampled points are obtained by using the permutations of the original sample. To speed up the fluttering process, in both runs the eel is set into a pre-bent shape prior to the beginning of each simulation. The investigated physical system is then simulated in a 0.1 s time period, with an average computational time of 3 h per sample. After the model is learned, sensitivity analyses are performed by using derivative and variance sensitivity methods. As a result, in the first run the highest influencing indices are obtained for length L, while radius R has a lower influence and distance d the lowest. In the second run, parameter L is still the most influential, followed, however, by d and only then by R, with an order of magnitude difference between the influence of L and the other two parameters. The interrelated contribution of the input parameters is also to be considered, and it is thus established that in the first run case the d-L, d-R and R-L relations are important, as are the d-L and R-L interconnections in the second run. Finally, for the first run the optimal values for R, L and d are established as: 0.2 m, 0.24 m, and 0.02 m, while for the second run the optimal values are, respectively, 0.21 m, 0.46 m and 0.2 m [25].

Since the models allowed constraining the domain of values of eel's design parameters, of bluff body dimensions and distances between the bluff body and the eel, aimed at maximising the respective output voltages, a prototype eel could be designed so as to gain insight into the dynamics of the investigated device. Eel's design, modified in agreement with the company chosen for its manufacture, that has extensive experience in piezoelectric films [27], so as to include changes in the substrate material, the electrode patterns and the watertight encapsulation, is thus depicted in Fig. 4. The assembly (Fig. 4a) consists thus finally of 13 layers:

- a central substrate Mylar® layer (t_s = 125 μm) – designated in Fig. 4a with 1;
- two active piezoelectric PVDF layers (t_{PVDF} = 110 μm) annealed at 60 °C and plasma etched to ensure better adhesion of the electrodes – designated with 3;
- four ultra-thin screen-printed conductive silver ink electrode layers in the form of totally 16 electrodes (8 positive and 8 negative) – designated with 2 (see also Fig. 4b);
- two outer protective Mylar® layers (t_p = 25 μm) that ensure a watertight enclosure of the device – designated with 4,
- and four pressure sensitive epoxy layers (t_{ep} = 10 μm) in-between the PVDF and the Mylar® layers.

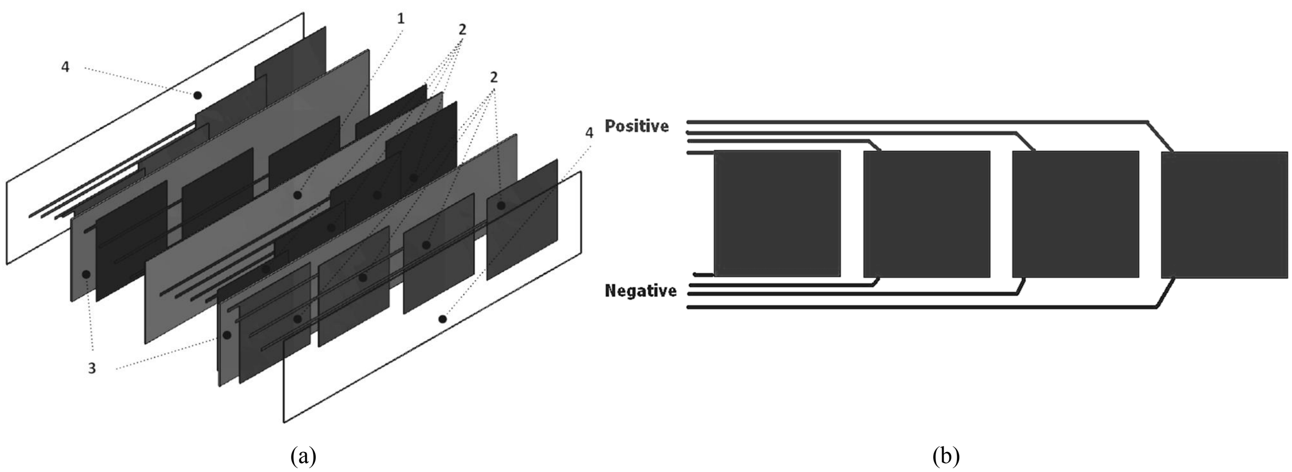

Figure 4. CAD model of the piezoelectric eel assembly (a) and the corresponding silver ink electrode pattern of a single PVDF layer with four electrode pairs (on top of the PVDF layer with positive and on the bottom with negative electrodes).

Figure 5. Manufactured eel prototype with indicated electrode segments (a) and eel's cross section with an indication of the outer protective PET layers (1), of the epoxy layers (2), of the PVDF layers (3) and of the substrate PET layer (4) (b).

The finally manufactured prototype, having a total length of L = 621 mm, is shown in Fig. 5a where a layer of the four silver ink electrode patterns are clearly visible. As shown in Figs. 4b and 5a, to ensure charge collecting at the most convenient locations, each of the total number of 16 electrodes (four electrodes on each side of the two PVDF layers) requires a collector (drain) leading out to one of the solder tab crimped contacts at the clamped end of the eel to be mounted close to the bluff body. Due to the positioning of drains, the actual ell's assembly is broader in width with respect to the nominal size, and measures w = 194 mm. A potentially bigger number of electrode segments would further increase eel's width and make the device somewhat impractical when considering the downstream electric circuit connections but, on the other hand, it would also increase the obtained powers due to less voltage cancelations owing to the fluttering shapes of the eel during its operation (see also below). What is more, although the nominal device thickness is $t_T \approx 435$ μm, the actual thickness measured on the manufactured prototypes by using a stereomicroscope (Fig. 5b) is in average around 450 μm. This is due to the manufacturing tolerances on the thickness of the various layers constituting the eel assembly and irregularities (partial delamination and captured air bubbles) that occurred during the manufacturing process itself.

The availability of the prototypes allows also measuring the composite Young's modulus of the whole ell's assembly, needed for better tuning the numerical models and interpreting the experimental results. For this purpose, a tensile universal testing machine, Shimadzu Autograph AGS-X [28], available at the Laboratory for Precision Engineering and Micro- and Nanosystems Technologies of the Centre for Micro- and Nano-Sciences and Technologies of the University of Rijeka, Croatia, is employed. This testing machine is equipped with a 5 kN range load cell having a resolution of 10 N, while the resolution of the respective extension measurement device (i.e. of the elongation ε of the sample) is 10 μm. One of the eels is hence sacrificed and cut into 200 x 20 mm bands that are placed between wedge grips of the tensile machine. A static load test is then performed allowing to determine that the composite eel's material exhibits a linear stress-strain behaviour up until $\sigma_{0.2} \approx 40$ MPa with a Young's modulus of E ≈ 3.5 GPa, as well as that the ultimate tensile strength of the eel is at $\sigma_M \approx 186$ MPa (Fig. 6).

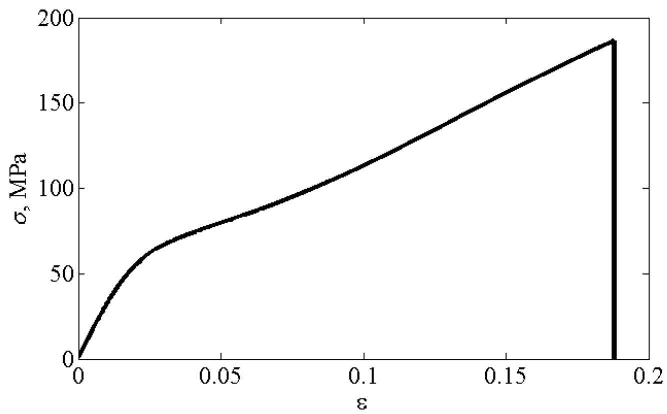

Figure 6. Stress-strain curve of the static load test performed on eel's composite assembly material.

2.3 Hybrid piezoelectric plucking concept

The third concept proposed in this work is based on a rigid piezoelectric cantilever bimorph periodically 'plucked' (i.e. periodically struck) by 'plectra' mounted on the shaft of the hydro-generator (Fig. 1c) and then allowed to vibrate freely thus converting, via the direct piezoelectric effect, the transient mechanical response of the vibrating beam into electric charges in the piezoelectric layer. In the conceived configuration, the piezoelectric cantilever is clamped on the inner side of the housing of the generator and orientated perpendicular to the rotation axis of the shaft that hosts several fulcrums protruding radially from it (Fig. 7).

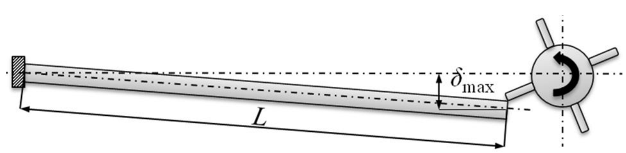

Figure 7. Scheme of a piezoelectric cantilever of length L struck by a fulcrum protruding from hydro-generator's shaft.

In order to obtain a first-order approximation of the power obtainable from the transient response of a piezoelectric bimorph cantilever, in this work a single impact, producing cantilever's deflection δ, is studied numerically by employing finite element modelling (FEM). A river flow speed of v_r = 1 m/s is assumed, while the propeller geometry is that used in the DC hydro-generator of section 2.1., thus resulting in a rotational frequency of 250 rpm (c.f. also Fig. 11b). An off-the-shelf Midé Technology® Volture cantilever energy scavenger, model V21b, is considered (c.f. [13]), wherein the maximum dynamic tensile strength of the PZT-5A ceramic piezoelectric layers, that delimits the maximum allowable deflection δ_{max}

of the cantilever, is σ_{M_dyn} = 27.6 MPa [29]. By employing simple strength of materials first-order calculations to determine the corresponding allowable forces to be applied at the free end of the cantilever, and taking into account a 20 % safety factor, a value of F_{max} = 0.765N is obtained, thus implying a δ_{max} =0.32 mm maximal deflection (Fig. 7). Given this value and considering the rotational frequency of shaft's axis, an approximate impact time, i.e. the time while the fulcrum is in contact with the cantilever, is calculated to be t_i = 0.35 ms.

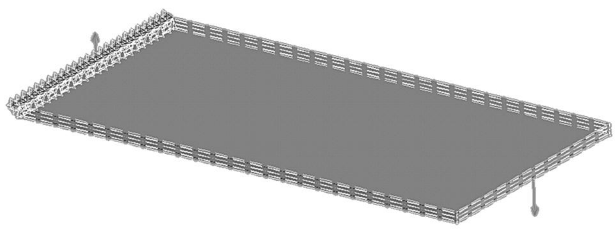

(a)

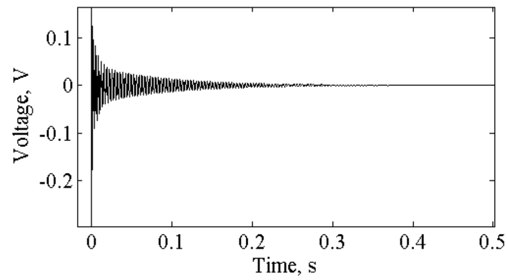

(b)

Figure 8. Numerically modelled Midé® Volture V21B scavenger (a) and corresponding transient response resulting from impact force loading (b).

The FEM simulation is set-up in the ANSYS® software package (Fig. 8a) as a transient analysis that is thoroughly described and experimentally verified in [13]. In this particular case, the excitation profile is then, obviously, adjusted to the single impact at the free end of the cantilever that is modelled as a ramped load F_{max} lasting exactly for the calculated time t_i, to be then instantly released inducing the free vibration transient response of the cantilever (Fig. 8b). The piezoelectric layers are connected in the model in a series electrical circuit coupled with an R_l = 100 Ω resistor. This value is chosen so as to simulate the internal electrical resistance of the downstream loads (i.e. the energy management electronics of section 3). Results of the performed simulations show that a small ($U \approx$ 0.27V) voltage is generated from the single impact. This value cannot overcome the threshold voltage limit required for the supply of energy to the management electronics described in following section. Further numerical and experimental investigations, considering several plectra and the inclusion of a larger number of piezoelectric cantilevers being concurrently struck by shaft's protrusions, are hence planned.

3. ENERGY MANAGEMENT ELECTRONICS

While by using the hydro-generator, DC voltage, with an amplitude dependent on river flow velocity, is generated, the piezoelectric eel and the hybrid energy harvesting concepts generate random voltage amplitudes. The obtained energy must therefore be properly managed to achieve DC voltage levels compatible with the used sensors and the respective electronics [14]. The main purpose of this circuitry is to reduce and stabilize the voltage levels to a value of 5 V (or, alternatively, 3.3 V) to be used for powering the sensor cluster's electronics. On the other hand, excessive energy is to be stored on a supercapacitor and used as a power source when higher power bursts are required by the communications module. A suitable energy management electronics, based on a Fujitsu Semiconductor integrated circuit [30], is hence designed, manufactured and used in all the performed experiments (see sections 4 and 5 below). The list of the used electrical elements in this frame is given in Table 2, while the electrical scheme and the manufactured PCB are shown in Fig. 9.

Table 2.Specification of the elements of the energy management electronics.

Chip	C_1	C_2 (supercapacitor)	C_3
Fujitsu MB39C811	10 μF	50 F	4.7 μF

It is to be noticed here that the harvester is to be integrated within a sensor node system that has a backup battery; internal logic then switches the battery on and off depending on energy consumption. When the battery is triggered, the supercapacitor is charged to 4.6 V; the battery is hence switched off. From that point on, the discharging of the supercapacitor is replenished by the charge produced by the harvester device, up until the voltage on the supercapacitor is above 3.6 V. Only when the voltage drops below this threshold, i.e. when the energy generated by the harvester is not sufficient to cover consumption, the battery is turned on again topping-up the deficit of energy given by the difference of that produced by the harvester and that drawn by the electrical loads.

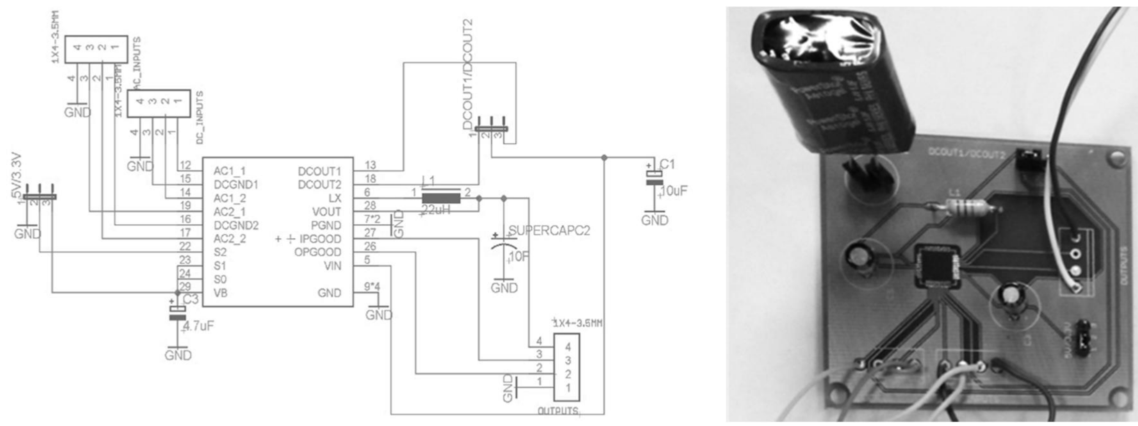

(a) (b)

Figure 9. Scheme of energy management electronics (a) and PCB with all electrical elements (b).

4. LABORATORY EXPERIMENTS

Based on the above consideration, laboratory experiments were set-up for the miniaturised DC hydro-generator and the piezoelectric eel energy harvesting concepts. An experimental flow tunnel with a suitable volume, that enables a controlled variation of water flow velocities while allowing for concurrent measurements of the voltages produced by the harvesters, is available at the Naval Research Institute in Zagreb, Croatia [31], where it is generally used for measuring cavitation effects on propeller blades. The test segment of the tunnel is long 2.2 m while its active cross-section is 0.5 x 0.5 m and it is suited to produce maximal flow velocities of up to 8 m/s with minimum increments of 0.25 m/s. Appropriate interfaces for the individual harvester test beds and the electrical feedthroughs leading out of the chamber were prepared by the staff of the Institute. The hydrometric screw turbines' wings-based sensors are used to attain stable flow velocity measurements, one at the beginning of the test segment and one at its end. All the control and regulation components of the Institute's system are then interfaced to an apposite National Instruments data acquisition system.

4.1. Experiments with the miniaturised hydro-generator

With the configuration of the miniaturized DC generator described in section 2.1. of this work, a set of experimental measurements is hence performed (Fig. 10) with the aim of investigating its behaviour in controlled flow conditions. As depicted in Fig. 10b, the miniaturized hydro-generator is hence fixed to the flow tunnel via a suitable support and tested within a flow velocity range of up to 4 m/s continuously increased in a relatively short time span.

(a) (b)

Figure 10. Flow tunnel at the Naval Research Institute in Zagreb, Croatia (a) and underwater hydro-generator rotating in the tunnel (b).

Although the nominal voltage of the generator is 18 V, in the first set of the experiments much higher voltages are purposely produced to attain the voltage vs. flow velocity characteristic in the entire considered velocity range (Fig. 11a). The obtained curve can then be easily scaled up or down depending on the gearhead mounted on the generator. The corresponding dependence between flow velocity and rotational speed of the propeller is shown in Fig. 11b.

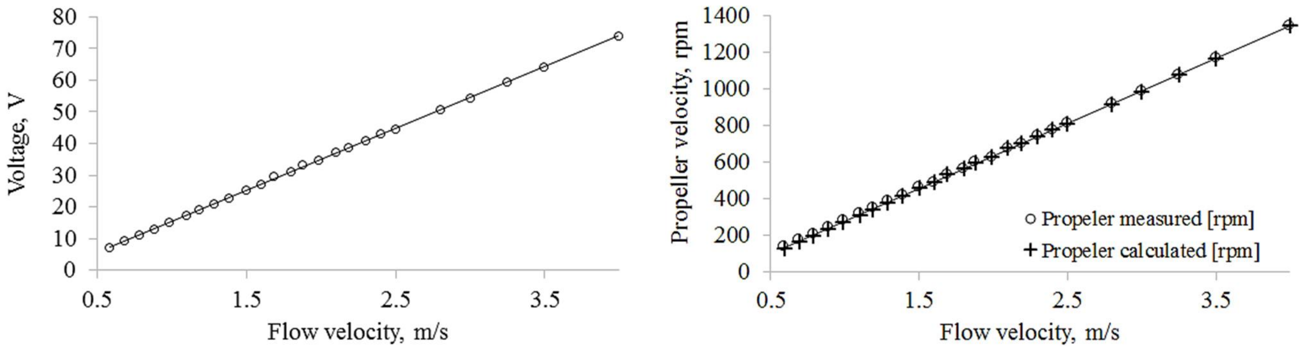

(a) (b)

Figure 11. Voltage of the DC generator (a) and rate of propeller rotation vs. flow velocity (b).

In the second set of experiments, the range of water flow velocities enabling propeller rotation of the miniaturised DC generator is established. It is thus determined that propeller rotation starts at flow velocities higher than 0.59 m/s and then stops when the velocity drops below 0.37 m/s. This behaviour is directly related to the Stribeck frictional effect: once the static friction torques at the motor windings, bearings and other components is overcome and rotation starts, the torque needed to perpetuate the rotation drops to a value compatible with dynamic frictional components. Obviously, the flow velocity threshold at which the propeller starts to rotate depends also on the type of the propeller. The same experimental set-up allowed in fact confirming that, when the propeller with wider blades, i.e. with a larger effective area is used, its rotation is initiated at lower flow velocities.

Most importantly, the experiments at the Naval Research Institute's facilities allowed establishing that the developed hydro-generator harvester enables power levels at the turbine (i.e. at the input into the harvester system) of $P_{\mathrm{in}} \approx 700$ mW to be generated. On the other hand, the measured voltages and currents on a 'dummy load' composed of successfully powered LEDs (simulating the sensors cluster) correspond to generator's output powers of up to $P_{\mathrm{out}} \approx 220$ mW [6].

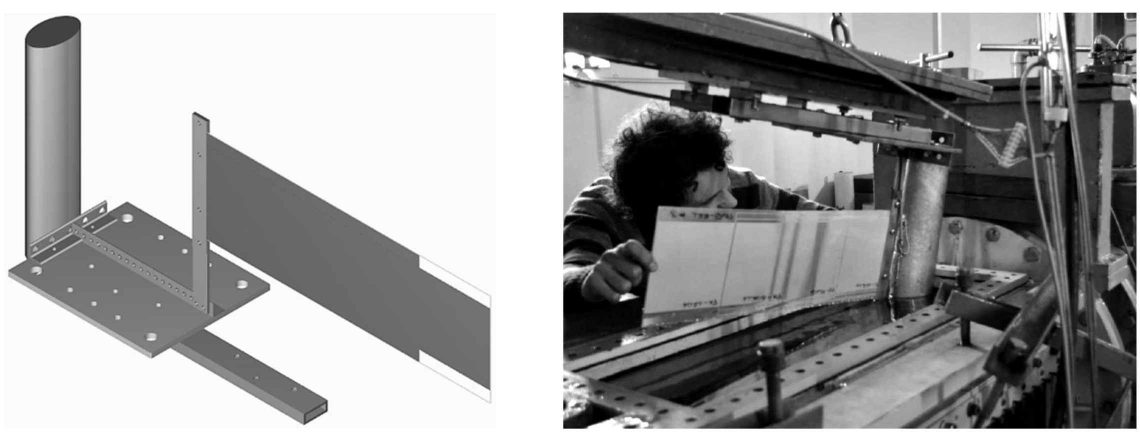

(a) (b)

Figure 12. Piezoelectric eel test bed (a) and eel mounting process at the Naval Research Institute with a tubular bluff body mounted behind the eel (b).

4.2. Piezoelectric eel experiments

To assess the piezoelectric eel's dynamic behaviour and to determine a practical eel's design parameter range that would enable its operation in real river conditions, following the piezoelectric eel design thoroughly explained in section 2.2. of this work, experiments are performed at the Naval Research Institute's facilities described above. Four variables are particularly monitored as the most relevant ones: bluff body shape, its size, distance of the eel from the bluff body and flow speed. A suitable test bed, allowing bluff body exchange and repositioning of the eel, is hence designed and manufactured (Fig. 12a). Two different shapes of bluff bodies are thus used, each with three different widths: tubular bodies with external diameters of ϕ = 100, 150 and 200 mm and plates with corresponding W = 100, 150 and 200 mm widths. Three considered eel-to-body distances are d = 40, 80 and 120 mm, while the flow speed is varied in the range v_r = 0.5-2 m/s with 0.5 m/s increments. Each of the four electrode segments of the eel (c.f. Fig. 5a) is separately connected in a parallel electrical circuit (i.e. the top outer electrode is connected with the inner bottom electrode, while the top inner electrode is connected with the outer bottom electrode of the segment) so as to produce greater electric currents. In fact, since, as previously stated, the PVDF material can produce large electric charge magnitudes, a series connection is not necessary, while larger current values, which may enable a more efficient functioning of the downstream electrical loads, are aimed for. The resulting exposed soldered connections at eel's tail are then protected from the water by using a two-component epoxy. At that point, each of the four separate parallel connections is attached to an oscilloscope via the feedthrough leading out from the top window of the test chamber. The piezoelectric eel has in any case to be taken out of the flow tunnel for each experimental run by employing a portal crane, so as to enable bluff bodies and/or eel's positions to be altered (Fig. 12b). A total of 280 AC RMS voltage measurements are finally performed with additional repeatability checks of the values at determined flow velocities. In general, the flow tunnel proved to be too narrow, especially when larger bluff bodies are used with flow velocities v_r < 1 m/s, thus hindering the occurrence of regular von Karman vortexes. This is especially noticeable when plate-shaped bluff bodies are used, inducing an under-pressure just behind them that cause the eel to twist and bend back towards the bluff body, eventually breaking down (Fig. 13a). The largest experimentally obtained voltages are achieved at a flow velocity $v_r \approx$ 1-1,5 m/s when the largest tubular bluff body ϕ = 200 mm, at a distance between it and the eel of $d \approx$ 100 mm, is used; tendentiously, for smaller bluff body diameters, the eel has to be moved slightly towards it. The oscillatory shape of the eel in this condition is quasi-sinusoidal (Fig. 13b).

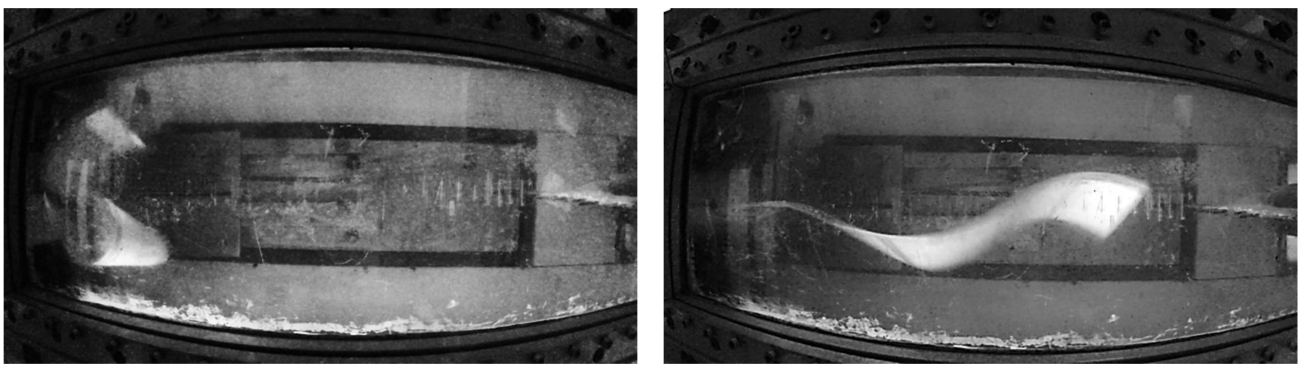

(a) (b)

Figure 13. Piezoelectric eel during the experiments: eel bent and twisted all the way back towards the plate-shaped bluff body (a) and quasi-sinusoidal shape of the eel membrane when a tubular bluff body is used (b).

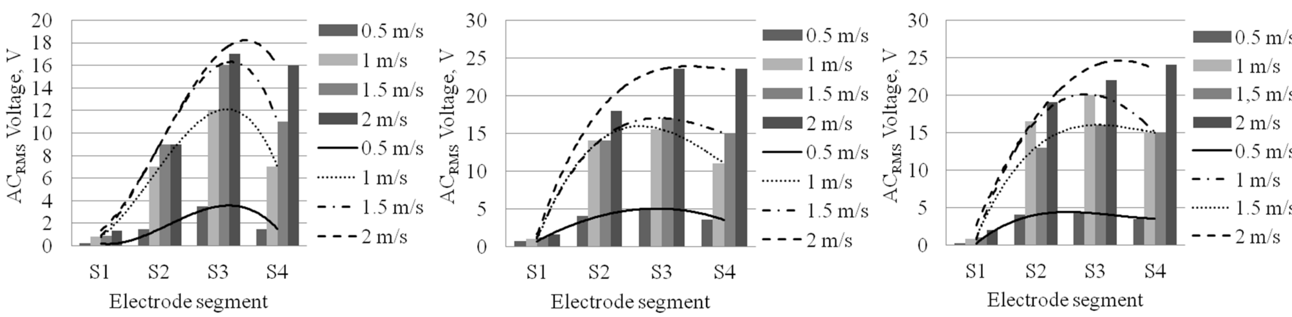

(a) (b) (c)

Figure 14. Piezoelectric eel voltages per electrode segments and variable flow velocities when employing a ϕ = 200 mm bluff body with d = 40 mm (a), d = 80 mm (b) and d = 120 mm; trend lines are shown as respective eel's 'pseudo shapes'.

A more exhaustive scrutiny of the highest produced voltages is possible by observing the diagrams of Fig. 14. The case of the ϕ = 200 mm tubular bluff body at three eel's distances d and four flow velocities v_r (bearing in mind that the data for

$v_r \approx 2$ m/s are not reliable due to vicinity of the walls of the flow tunnel), is shown here. It is thus evident that the highest voltages are produced, longitudinally, in the 2nd (S2) and 3rd (S3) of eel's segments of Fig. 5a, with a close voltage magnitude also in the 4th segment (S4 – eel's 'head'), while the 1st segment (S1 – eel's 'tail') is basically inactive, which can be attributed to the clamping of the eel's tail. The corresponding polynomial curves shown in Fig. 14 represent the 'quasi steady state' eel's shapes achieved while recording the voltage values at corresponding flow velocities.

In any case, the resulting maximal AC output RMS voltages for the whole eel reach $U_{max} \approx 30$ V. Based on the resulting supercapacitor's charging periods, the corresponding output power can be estimated to be in the $P \approx 10$ mW range. The overall power could ultimately be enhanced by using several eels.

5. RIVER EXPERIMENTS

Real river-flow field experiments are finally carried out with the miniaturised DC turbine energy harvesting solution, i.e. the one guaranteeing the highest energy production, at two different rivers, the Rječina river near Rijeka, Croatia and the Liewec river near Warsaw, Poland. The conditions during the field measurements for the both rivers are given in Table 3.

Table 3.Conditions during field measurements.

River	Depth at the position of the experiment	Distance of the axis of the turbine from the river bed	Flow velocity at the axis of the turbine
Rječina	0.5 m	0.3 m	1 m/s
Liewec	0.6 m	0.32 m	0.64 m/s

During the first set of field experiments performed at the Rječina river in Rijeka, Croatia, the velocity of the river flow is estimated to be $v_r \approx 1$ m/s. This is established by measuring repetitively (> 10 times) the time necessary for a piece of Styrofoam on river's surface to cover 10 meters. The underwater hydro-generator experiments are then performed with the mentioned LEDs' 'dummy load' attached at the output of the management electronics described in section 3 of this work. It could thus be confirmed that, at the input into the harvester system, a power of $P_{in} \approx 700$ mW (c.f. section 4.1.) is generated, while, depending on the loads, at system's output powers in the range $P_{out} \approx 115$-500 mW are obtained [6].

The final river-flow field experiments are conducted at the Liewec river in Warsaw, Poland, where the miniaturised turbine harvester is integrated with the real pollution monitoring system (Fig. 15). In this, case, the river flow is precisely measured at the position of harvester's deployment by employing a suitable water stream flow-rate current meter.

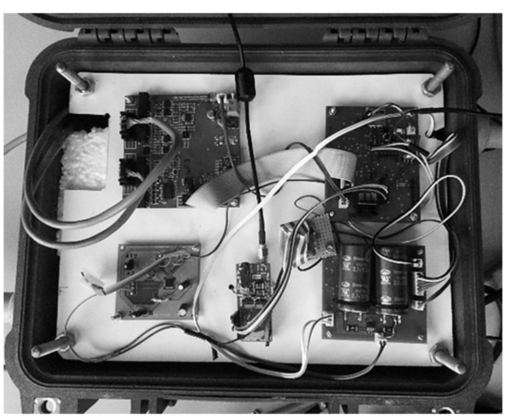

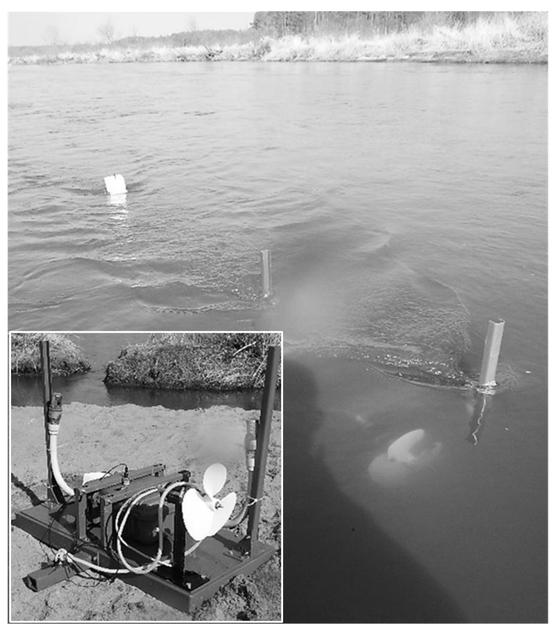

Figure 15. Integrated sensor node electronics (a) and experiments at the Liewec river, Warsaw, Poland (b).

In all the experiments, the measurement and controller boards are set to collect the data from the sensors every 15 s while the time needed for measurements is one second. The communications module used to deliver the data to the gateway located on the riverbank needs 2 minutes to successfully transmit the data and is set to operate once every hour. It could thus be shown that, for the hence defined working periods and without using a battery, the miniaturised hydro-generator harvester can successfully power the control and measurement boards, accomplishing thus the main goal of the project. However, since the entity of the river flow velocity at the position of the experiments is an essential boundary condition for the developed harvester, it could not yet be unquestionably confirmed that the charging of the communications module, attained during its sleep mode, can withstand its transmission activity. In order to definitely exclude this last doubt, a further set of filed experiments with the integrated sensor node system will be repeated in the river where the system will be finally operated and that certainly has flow velocities well above the threshold guaranteeing the most efficient performances of the hydro-generator harvester.

6. CONCLUSIONS AND OUTLOOK

The conception, design and manufacturing of energy harvesting devices to be employed as a power source for pollution monitoring sensor clusters to be deployed in river streams is described in this work. Three energy harvesting concepts are proposed: a miniaturised DC hydro-generator, so-called piezoelectric eels and a hybrid solution as a combination of the other two concepts. Thorough modelling and calculations are performed to optimise the design of the foreseen harvesting devices as well as the respective energy management electronics. The underwater turbine and the piezoelectric eel concept are subsequently validated also experimentally. In a first instance, laboratory experiments are hence conducted in a suitable flow tunnel at the Naval Research Institute in Zagreb, Croatia. Besides establishing operational performance data, experiments with the hydro-generator allowed thus input powers of $P_{\text{in}} \approx 700$ mW and output powers of up to $P_{\text{out}} \approx 220$ mW, which corresponds to calculated values, to be generated. Consequently, a 'dummy load' composed of standard LEDs, simulating the sensor cluster, has been successfully powered. On the other hand, the pioneering piezoelectric eel is successfully prototyped. Material tests are performed, followed by dynamics tests in the same facilities of the Naval Research Institute. It is thus demonstrated that a single eel behind a $\phi = 200$ mm tubular bluff body can generate up to $P \approx 10$ mW. This overall configuration seems, however, to be in contradiction with the results of the numerical model results, indicating that additional comparative analyses are needed. In this regard, part of the discrepancies might be related to the simulated time limitation of the numerical model (0.1 s) determined by overall computational times, that are too short to capture the complete fluttering period of the eel; in fact, the experimentally seen fluttering frequencies are in the 1-3 Hz range. On the other hand, a significant limitation during the performed experiments is the small width of the flow tunnel that induces unwanted boundary effects.

In the final stages of the work, the DC turbine harvesting device and its management electronics are successfully tested in real fiver-flow conditions at the Rječina river near Rijeka, Croatia, powering again successfully the dummy loads and producing again power levels of, respectively, $P_{\text{in}} \approx 700$ mW and $P_{\text{out}} \approx 115$-$220$ mW. The harvester is hence integrated into the complete sensor node cluster and further field experiments are performed at the Liewec river in Warsaw, Poland. The underwater hydro-generator energy harvester design successfully powered the measurement and controller boards that are triggered every 15 seconds to collect the data from the sensors, realizing thus the main goal of the project. The developed hydro-generator and its energy management electronics will consequently be soon embedded into the final configuration of the wireless system aimed at tracking pollution in remote watercourses using sensor network technology.

ACKNOWLEDGEMENTS

The work presented in this paper is part of and is supported by the EU FP7 ICT-2009.9.1 project no. 269985 "GOLDFISH – Detection of Watercourse Contamination in Developing countries using Sensor Networks – Enlarged".

REFERENCES

[1] GOLDFISH EU FP7 ICT-2009.9.1 project no. 269985, "Detection of Watercourse Contamination in Developing Countries using Sensor Networks - Enlarged, Annex I - Description of work" (2013).

[2] Erturk, A. and Inman, D., [Piezoelectric energy harvesting], John Wiley & Sons, Chichester (2011).

[3] Kazmierski, T. and Beeby, S. (ed.), [Energy Harvesting Systems: Principles, Modeling and Applications], Springer, New York (2011).

[4] Priya, S. and Inman, D. (ed.), [Energy Harvesting Technologies], Springer, New York (2009).

[5] Mateu, L. and Moll, F., "Review of Energy Harvesting Techniques and Applications for Microelectronics," Proc. SPIE 5837 – VLSI Circuits and Systems II, 359-373 (2005).

[6] Kamenar, E., Gregov, G., Zelenika, S., Blažević, D. and Marković, K., "Miniaturized underwater hydro generator for powering wireless sensor network nodes," Proc. 24th Int. Con. Energy & Environ., Opatija, Croatia (2014).

[7] Allen, J. J. and Smits, A. J., "Energy harvesting eel," J. Fluids & Struct. 15/3-4, 629-640 (2001).

[8] Carrol, C. B, "Energy harvesting eel," US Patent 6,424,079 B1 (2002).

[9] Doare, O. and Michelin, S. "Piezoelectric coupling in energy-harvesting fluttering flexible plates: linear stability analysis and conversion efficiency," J. Fluids Struct. 27/8, 1357–1375 (2011).

[10] Taylor, G. W., Burns, J. R., Kammann, S. M., Powers, W. B. and Welsh, T. R., "The Energy Harvesting Eel: A Small Subsurface Ocean/River Power Generator," IEEE J. Oceanic Eng. 26(4), 539-547 (2001).

[11] Techet, A. H., Allen, J. J. and Smits, A. J., "Piezoelectric Eels for Energy Harvesting in the Ocean," Proc. 12th Int. Offshore & Polar Eng. Conf., Kitakyushu, Japan (2002).

[12] Pozzi, M. and Zhu M., "Plucked piezoelectric bimorphs for energy harvesting applications," Proc. SPIE 8066 – Smart Sens., Act. & MEMS V, 806616 (2011).

[13] Blažević, D. and Zelenika, "Nonlinear numerical modelling and experimental validation of multilayer piezoelectric vibration energy scavengers," these proceedings.

[14] Zelenika, S., Kamenar, E., Maćešić, S., Blažević, D., Gregov, G. and Marković, K., "Design and specification of the energy harvesters and underwater harvester anchorage," Deliverable 4.4. of the EU FP7 ICT-2009.9.1 project no. 269985 GOLDFISH, Rijeka, Croatia (2014).

[15] Zelenika, S., Kamenar, E., Maćešić, S., Blažević, D., Gregov, G., Marković, K. and Glažar, V., "Complete laboratory functionality of at least one variant of the energy harvester," Deliverable 4.5. of the of the EU FP7 ICT-2009.9.1 project no. 269985 GOLDFISH, Rijeka, Croatia (2014).

[16] ‹https://fmcc.faulhaber.com/type/PGR_13813_13801/PGR_13818_13813/en/GLOBAL/› (March 2014). fmcc.faulhaber.com/type/PGR_13813_13801/PGR_13818_13813/en/GLOBAL/

[17] ‹http://www.stratasys.com/3d-printers/design-series/fortus-250mc› (March 2015). www.stratasys.com/3d-printers/design-series/fortus-250mc

[18] Akcabay, D. T. and Young, Y. L., "Hydroelastic Response and Energy Harvesting Potential of Flexible Piezoelectric Beams in Viscous Flow," Phys. Fluids 24, 054106 (2013).

[19] Gao, X., Shih, W.-H. and Shih W. Y., "Flow Energy Harvesting Using Piezoelectric Cantilevers With Cylindrical Extension," IEEE Trans Ind. Electr. 60/3, 1116-1118 (2013).

[20] Wang, D.-A., Chiu, Ch.-Y., Pham, H.-T., "Electromagnetic energy harvesting from vibrations induced by Kármán vortex street," Mechatronics 22/6, 746–756 (2012).

[21] Wu, Y.-J. and Lai, W.-H., "Simulation of piezoelectric jellyfish power generator," Mod. Phys. Lett. B24/13, 1325-1328 (2010).

[22] Measurement Specialties, [Piezo Film Sensors Technical Manual], Hampton (2008)

[23] Kim, Y. and Peskin, C. S., "Penalty Immersed Boundary Method for an Elastic Boundary with Mass," Phys. Fluids 19, 053103 (2007).

[24] AIMdyn Inc., Santa Barbara (CA, USA), ‹https://aimdyn.com› (January 2015). aimdyn.com

[25] AIMdyn Inc., [Report on the sensitivity and optimization results obtained by the GoSUMD software to maximize the produced voltage by piezoelectric eel], AIMdyn Inc., Santa Barbara (CA, USA), March (2015).

[26] Abramson, M. A., Audet, C., Chrissis, J. W. and Walston, J. G., "Mesh adaptive direct search algorithms for mixed variable optimization," Opt. Letters 3/1, 35-47 (2009).

[27] ‹https://www.meas-spec.com/› (October 2014). www.meas-spec.com

[28] ‹http://www.ssi.shimadzu.com/products/literature/Testing/C224-E057.pdf› (February 2015). www.ssi.shimadzu.com/products/literature/Testing/C224-E057.pdf

[29] ‹http://www.morganelectroceramics.com/resources/piezo-ceramic-tutorials/typical-properties/› (April 2015). www.morganelectroceramics.com/resources/piezo-ceramic-tutorials/typical-properties/

[30] ‹http://www.fujitsu.com/sg/news/pr/fmal_20130513.html› (February 2014). www.fujitsu.com/sg/news/pr/fmal_20130513.html

[31] ‹http://www.hrbi.hr/index.php/en/› (July 2014). www.hrbi.hr/index.php/en/